ISFA2022-056

ADDITIVE MANUFACTURING OF BEAD-ON-A-STRING STRUCTURES USING NEAR-FIELD ELECTROSPINNING

Sanjana Subramaniam, Jian Cao, Kornel Ehmann¹
Northwestern University
Evanston, IL, USA

ABSTRACT

Near-field electrospinning (NFES) electrohydrodynamic (EHD) technique that presents a unique opportunity for the precise direct writing of 3D micro- and nanostructures using a wide array of compatible materials. which can be additively deposited through layer-by-layer stacking. The aim of this paper is to explore the controllability of beads-on-a-string (BOAS) structures through NFES using dilute high molecular-weight polymer solutions to print. As the BOAS morphology and deposition are highly dependent on the solution properties and the deposition process parameters, the influence of the solution's molecular weight and concentration, substrateneedle/nozzle spacing, substrate moving speed, and applied voltage that will enable the process control needed to obtain stackable beads with controllable spacing and area will be explored. The obtained results will expand upon the knowledge required for efficient process design for generating electrospun BOAS micro-and nanostructures with arbitrary and complex geometries as an additive manufacturing technique for applications in many fields.

Keywords: electrospinning, near-field electrospinning

1. INTRODUCTION

Electrospinning is a versatile, cost-effective process that uses an electric field to transform polymer solutions into nanoand micro-fibers. Its tunability and affinity for creating structures with high surface area to volume ratios and porosity have allowed it to be used in a wide variety of applications, such as filtration systems, tissue engineering and regenerative medicine, energy storage and harvesting devices, and microelectronics [1-3]. However, traditional electrospinning, which uses high voltages and large needle-to-collector distances, offers minimal control of the final morphology of the fibers. Conversely, near-field electrospinning can achieve greater controllability of fiber structure as it uses a reduced needle-to-collector distance (0.5 -

¹ Contact author: k-ehmann@northwestern.edu

5 mm) to avoid the whipping instability associated with its far-field counterpart (> 5 mm) and a programmable 3-axis stage to print fibers. It also uses low voltages (0 - 5 kV) and less polymer solution (< 2 - 5 mL), making it more economical. It offers many similar applications as traditional, far-field electrospinning, while offering a more tunable morphology [4-6].

morphologies can be achieved Several electrospinning, such as fibers, beads, beads-on-a-string (BOAS), and ribbons, by changing the solution, process, and environmental parameters. BOAS structures have mostly been overlooked and treated as an unwanted artifact due to their nonuniformity and decrease in surface area. However, they have gained more attention due to their unique wettability [7], hydrophobic [1, 8], tribological [9], drug delivery [10], and filtration [11] properties in far-field electrospinning. There are a few numerical studies on this topic, including one that maps polymer rheology to fiber morphology [12]. Some theoretical studies focus on the capillary breakup of viscoelastic filaments into BOAS structures [13-15], the effect of conductivity into the thinning of the viscoelastic liquid jet [16], role of surface tension on the development of BOAS structures in low viscosity, high molecular weight polymers [17], which have direct applications in BOAS formation in electrospinning.

There is comparably less exploration of the BOAS morphology in NFES. The theoretical studies of capillary break-up are relevant in the deposition in single-layer BOAS structures as the dilute long-chained polymer solutions deform in accordance with the Rayleigh-Plateau instability to minimize surface area while conserving volume. Single-pass BOAS were formed using alternating current fields under NFES conditions by varying the duty ration and AC voltage frequency [18]. Another study looked at the effect of conductivity and applied voltage to suspend vertical droplets of polyvinylpyrrolidone

(PVP) in glycerol and delved into the physics underlying this phenomenon [19]. They concluded that subsequent beads form when the previous one reaches the critical surface charge density at the Rayleigh limit. Moreover, this EHD printing technique has been used to pattern surfaces using direct current (DC) sources in a few experimental studies by varying process parameters such as solution concentration and substrate moving speed to obtain controllable sized beads in a single pass [20, 21]. However, this phenomenon has seldom been used as a manufacturing technique, besides one in a previous paper [22].

In this study, both the experimental variables that contribute to stackable beads as well as the physics that underlie the self-focusing behavior that enables the printing of multilayer structures are analyzed. The self-focusing mechanism (SFM) is essentially a not well understood attraction of a NFES polymer jet to previously deposited features, which allows for selective additive manufacturing of bead and bead-on-a-string structures in a layer-by-layer fashion.

This paper is organized as follows: The materials and methods are described in Section 2. Section 3 presents the experimental details that allow for BOAS deposition using NFES and analyzes the self-focusing mechanism (SFM) by determining the morphological changes that result from changing experimental parameters in order to control the process results. Finally, Section 4 has the conclusions and future outlooks of this work.

2. MATERIALS AND METHODS

An experimental set-up (Figure 1) was developed to perform NFES deposition. A 32-gauge stainless steel needle (Hamilton Company, 108 µm inner diameter, 235 µm outer diameter, 50 mm length) is attached to a high voltage power amplifier (Trek Model 10/10B-HS) that delivers positive DC voltages from 0 - 5 kV. The grounded substrate is a copper 110 plate (McMaster Carr), which is placed 5 mm away from the needle. It is also connected to a current pre-amplifier (Stanford Research Systems, SR570 Low Noise Current Preamplifier) to monitor the current flowing through the substrate. The substrate is placed on top of a 3-axis stage and motion controller (Aerotech ANT130XY & ATS100 Nanopositioning Stages), which can move in programmable patterns. The experimental set-up was placed in a controlled environmental chamber with a humidifier and a humidity and temperature probe (Vaisala HMP60) to ensure constant humidity. Experiments were conducted at room temperature and constant humidity.

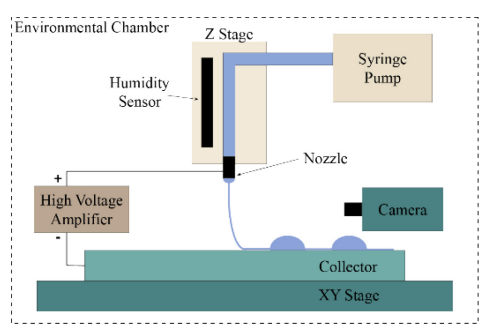


FIGURE 1: EXPERIMENTAL SETUP

Aqueous polyethylene oxide (PEO) solutions (Sigma-Aldrich) with varying molecular weights (20 kg/mol, 600 kg/mol, 4 Mg/mol) were prepared with several different concentrations (1 and 2 wt%) by dissolving PEO powder in deionized water overnight with a magnetic stirrer. PEO is a polymer frequently used in electrospinning for its versatility in the process. Several formulations of PEO, varying in molecular chain length and concentrations, are used to visualize the impact of solution chemistry in the BOAS printing process and gain a better knowledge of mapping solution characteristics to printed morphology. An Anton Paar MCR 301 Rheometer with a Couette fixture was used to determine the rheology of the PEO solutions. The electrical conductivity was determined using a conductivity meter (Thermo-Scientific).

The NFES process and jet behavior was recorded using a camera (Grasshopper GS3-U3-51S5M, 75 frames per second) with a variable magnification telecentric lens (Edmund Optics). A high-speed camera (FASTCAM Mini UX100 type 800K-M-16G, 4,000 frames per second) was also used to monitor the BOAS deposition process and evolution. The printed fibers were imaged using optical microscopy (Alicona G4 Infinite Focus optical microscope). A Zygo NewView 7300 light interferometer was used to evaluate the profiles of the BOAS fibers. Image-J was used to analyze the BOAS diameter. While Gwyddion was used to measure the heights of the BOAS structures.

The NFES deposition process was initiated by manually pumping the syringe pump until a droplet was formed on the tip of the needle. Constant pumping at 3.48 kPa was maintained throughout the deposition process. The high voltage supply was turned on and the droplet's surface tension was lightly broken with a tungsten probe, yielding a jet from the needle tip to the collector. The programmed motion of two 50 mm lines, separated by 10 mm, was started to print the BOAS structures. Once the motion was completed, pumping and the high voltage supply was stopped. Specifically in this paper, the influence of the solution molecular weight and concentration, as well as the substrate speed and number of passes was varied in order to elucidate the controllability of BOAS deposition in NFES.

3. RESULTS AND DISCUSSION

3.1 Characterization of PEO Solutions

The electrical conductivity of solutions at room temperature was determined (Figure 2). All measurements have a standard deviation of ± 0.1 . Note that the unit Dalton (Da) is equivalent to g/mol when referring to chain molecular weight. Generally, conductivity increases for more concentrated solutions. However, there is not a direct correlation among different molecular formulations of the same polymer, as there is not an obvious trend in conductivity measurements at a fixed concentration. For example, at the 0.5 wt% concentration, the conductivity readings are indistinguishable for the 4 MDa and 600 kDa formulations. Moreover, the conductivity measurements of the 600 kDa formulation are higher than those of the 4 MDa for increased concentrations, which makes it

unclear if there is exists an influence of molecular chain length on electrical conductivity.

Figure 3 displays the flow curves (i.e., viscosity vs. shear rate) for the 4 MDa PEO formulations. Shear rheology plays an influential role in the deposition process, as high shear rates are incurred in solutions as they pass through the electrospinning nozzle. Therefore, it is important to quantify this property. The smaller-chained PEO formulations, such as the 20 kDa and 600 kDa, displayed Newtonian behavior for all measured shear rates and are, therefore, neglected from Figure 3 for a lack of measurable viscoelastic behavior.

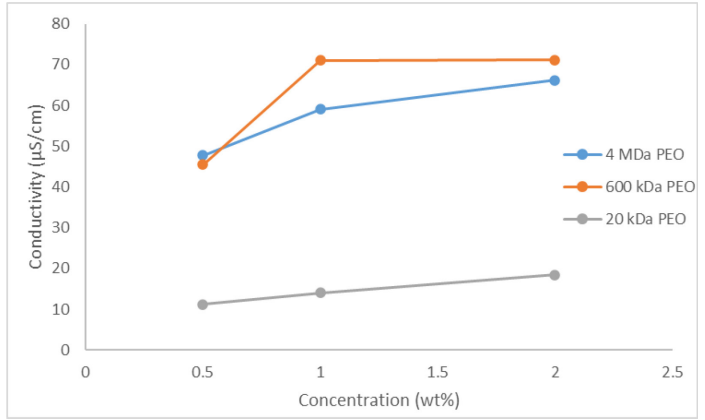


FIGURE 2: CONDUCTIVITY MEASUREMENTS

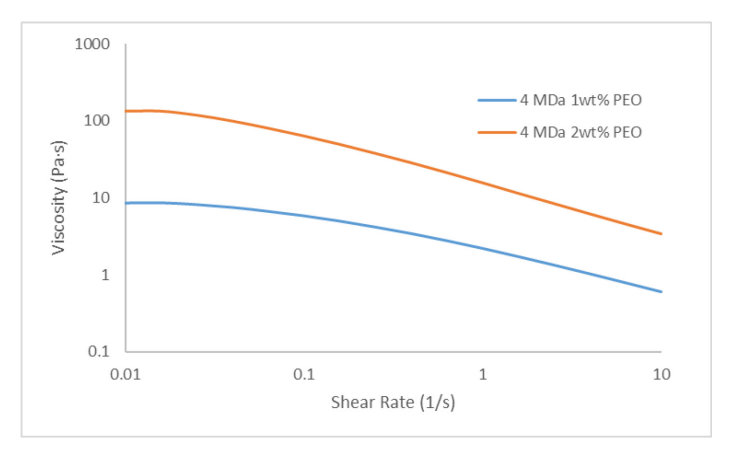


FIGURE 3: FLOW CURVES OF PEO SOLUTIONS

	Voltage (kV)		
Concentration (wt%)	20 kDa PEO	600 kDa PEO	4 MDa PEO
1	2.0	0.8	0.6
2	2.5	1.0	0.7

FIGURE 4: EMPIRICAL DETERMINATION OF SURFACE TENSION PROPERTIES IN THE ELECTROSPINNING PROCESS

Next, surface tension properties of the solutions were empirically determined by finding the minimum voltage required to initiate and sustain a stable electrospinning jet using constant pumping and a 5 mm substrate-to-collector distance (Figure 4).

All measurements have a standard deviation of ± 0.1 . More concentrated solutions and larger chained solutions require a lower voltage to create a jet. Using this data, a 2 kV high voltage supply was used for 1 wt% solutions and 2.4 kV for 2 wt% solutions to achieve stable jets for the printing process. Increased voltage will lead to thicker jets and prints, so it is important to use the lowest voltage possible in order to test the achievable resolution in this process.

3.2 Linear Pattern Deposition

Evaporation plays a crucial role in the development of stackable beads. Therefore, a programmable path (Figure 4) consisting of two 50 mm lines, separated by semicircles with 5 mm radii was developed. The size of the semicircular path was arbitrarily chosen as a safety measure so that no bead merging would occur among the two 50 mm lines. Any radius greater than the bead diameter would suffice. For repeated passes, it is important that the previous pass fully dries so that prints can build on top of one another in the direction perpendicular to the substrate without coalescence of adjacent beads. For this reason, a dwell time of 5 s was added to facilitate drying between passes which occurs at the same location as the start position. Also, a closed printing path ensures equal drying times for all beads. The prints during the semicircular toolpath were not analyzed in the subsequent parts of this paper as these were deposited at a variable acceleration, which will affect bead morphology and size.

For the process parameters, the substrate speed was varied from 25 - 125 mm/s in 25 mm increments and the number of passes was varied from 1, 2, 5, 10, and 20.

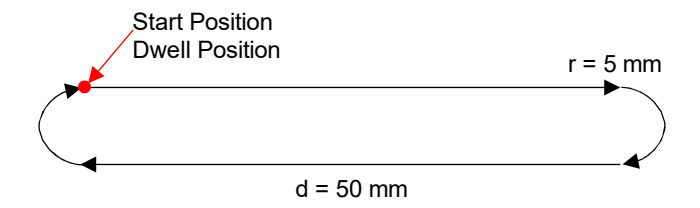


FIGURE 5: PRINTING PATH

3.3 BOAS Deposition and SFM Analysis

The deposited BOAS are shown in Figure 6 for the 4 MDa and Figure 7 for the 600 kDa formulation using a printing speed of 25 mm/s. Images of the 20 kDa solutions were omitted for brevity as they were identical in morphology to the 600 kDa solution results. This is likely due to their similar Newtonian behavior that deviates from the behavior of the 4 MDa PEO, which enables even spacing of discrete bead structures, rather than visible BOAS structures. The number of passes is denoted in each picture (ex: Fig. 6b.20 refers to the 2wt% 4 MDa formulation with 20 passes). The scalebars in Figures 6a.1 and 7a.1 denotes 200 and 100 μ m, respectively.

The presented images demonstrate the impact of solution properties (namely conductivity and viscosity) on the printed BOAS structures. Figure 6a shows BOAS structures printed with the 4 MDa, 1 wt% PEO solution. Successive passes cause a buildup of PEO solution on top of previously deposited beads, as

visualized in Figs. 6a.5, 6a.10, and 6a.20. However, the accumulation is non-linear, as seen in Fig. 6a.2, where successive passes are parallel to one another instead of printed on top of one another. The reason for this phenomenon is explained later in this section and is displayed in Figure 8.

For a larger number of passes, the above-described situation is more evident (Figs. 6a.10, and 6a.20). Bead stacking is not evenly spaced, nor is it evenly sized. It is hypothesized that this is caused by local charge buildup from previously deposited beads, which causes repulsion between subsequent passes. Therefore, the SFM attracts the jet to beads that were printed in previous passes. Charge buildup can be seen in Fig. 8, where the dots represent raw acquired current data from. The five different peaks correspond to 1, 2, 5, 10, and 20 passes. For a larger number of passes, charge accumulation is significant and contributes to the breakdown of the self-focusing mechanism.

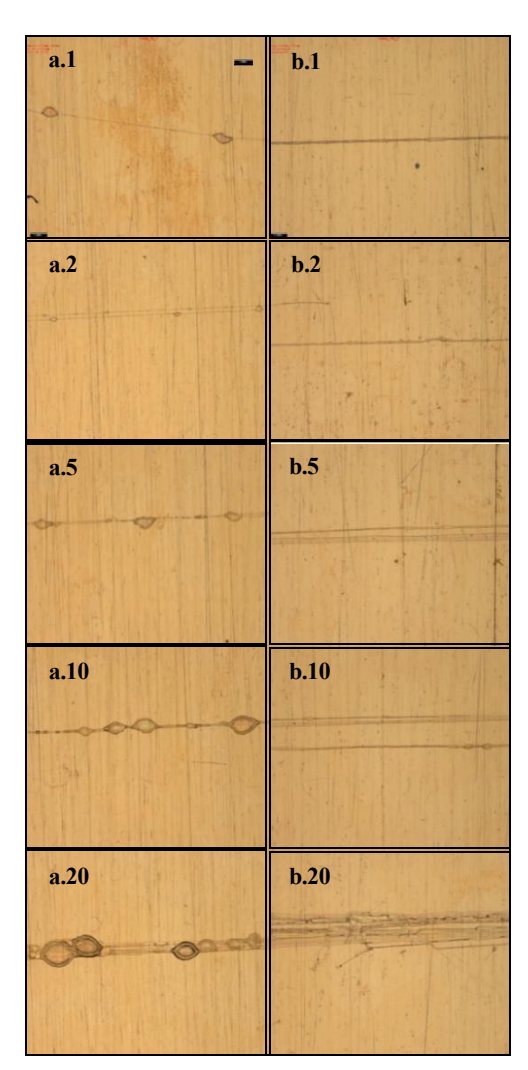


FIGURE 6: MULTILAYER PRINTS OF 4 MDA SOLUTIONS WITH 1WT% (FIG. 6A) AND 2WT% (FIG. 6B) FORMULATIONS

Using a smaller chained structure, such as the $600\,\mathrm{kDa}$ PEO solution, offers drastically different morphology. Instead of

BOAS structures, discrete bead structures are printed (Fig. 7a.1 and Fig. 7b.1). It is hypothesized that the filamented string structures either merged with the droplets or evaporated due to their large surface area. As more passes are deposited, the bead area increases. In the 1wt% formulation, with more than five passes, adjacent droplets merge to create droplets with larger areas or ribbons that look like one printed pass. This is undesired behavior as this merging creates larger droplet heights and decreased surface areas. Moreover, once larger droplets are created, their accumulated charge increases, meaning that the SFM will repel this deposited feature and create a parallel track (Fig. 7a.10 and 7a.20). This is slightly mitigated by using a more viscous formulation such as the 2wt% formulation, where the lower water content decreases the likelihood of merging droplets into a line with five successive passes (Fig. 6b.5). However, with more passes, adjacent droplets merge into a line, thus increasing again the charge accumulated and forcing the SFM to create a parallel pass of beads (Fig. 7b.20).

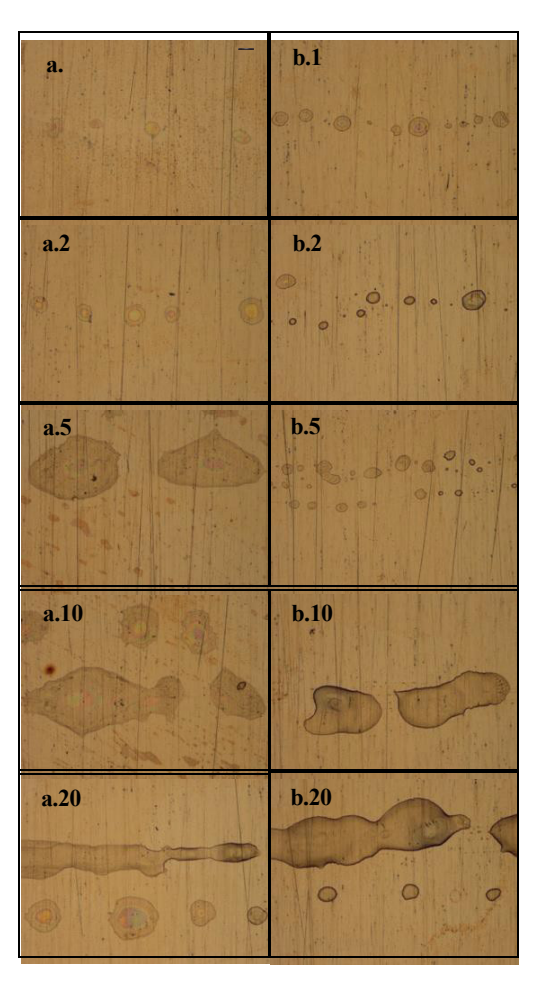


FIGURE 7: MULTILAYER PRINTS OF 600 KDA SOLUTIONS WITH 1WT% (FIG. 7A) AND 2WT% (FIG. 7B) FORMULATIONS

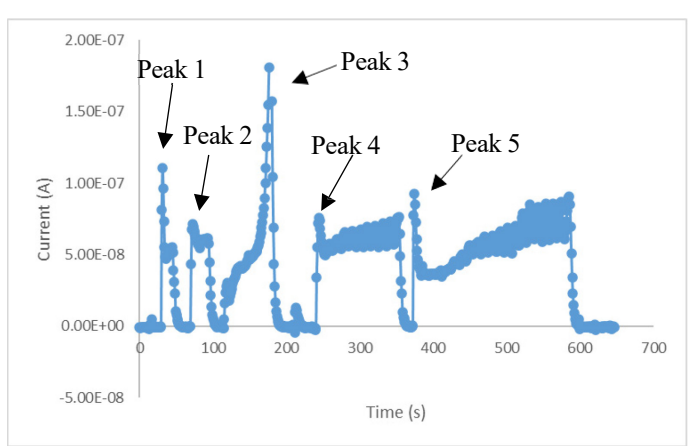


FIGURE 8: CURRENT EVALUATION AMONG MULTIPLE PASSES

3.4 BOAS Quantitative Size Analysis

The bead diameter, as defined as the length along the shorter, non-printing axis, and the bead height were quantified to analyze the impact of substrate speed and number of passes. The widths of the builds, or the length of the beads along the printing axis, were not quantified in this paper as it is difficult to decouple the inherent length without considering the effects of the drag forces inherent in the printing process that influence this parameter. These forces are more visible with higher substrate speeds. Note that the data from multilayer prints for the 4 MDa, 2 wt% solution are omitted as this print yielded no beads.

Figures 9 and 10 display data from multilayer prints printed at 25 mm/s. From these figures, it is evident that in general, increased passes have a positive influence on bead diameter and height, respectively, for all PEO formulations. The 20 kDa PEO solutions have the highest bead diameters and heights. It is hypothesized that this results from adjacent bead agglomeration, rather than stacking. Between different concentrations of the same PEO formulation, there is no significant difference in the bead diameter and height. However, Figures 6 and 7 demonstrate that the morphology of the beads varies drastically. There also seems to be stagnated values for bead diameter and height for an intermediate number of passes. This could be caused by local repulsions between subsequent passes, causing two parallel passes. This can be visualized through Figure 8, where there are spikes of current in the 2 pass and 5 pass trials. As the charge dissipates over time from the initial transient spike, the selffocusing mechanism becomes more evident; the bead diameters and heights for the 10 and 20 pass trials increase from that of the intermediary passes. The only exception for this trend is in Figure 9, for the 20 kDa, 1 wt% solution.

Figures 11 and 12 display data from the multilayer prints of 600 kDa, 1 wt% PEO formulation. As substrate speed increases, the bead diameter and height decreases. It is theorized that this is caused by a shorter time window for the self-focusing mechanism to deposit material on top of each bead. At each value of substrate speed, there generally seems to be an increase in bead diameter and height as the number of passes increases. Another interesting finding is that the bead heights and diameters for the 20 pass runs are lower than the 5 or 10 pass runs. This is

likely due to adjacent bead agglomeration or multiple parallel passes, which cause bead diameter and height to decrease.

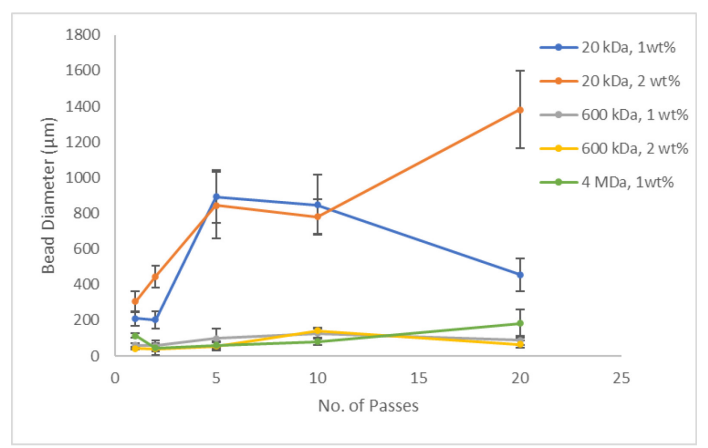


FIGURE 9: INFLUENCE OF PASS COUNT ON BEAD DIAMETER

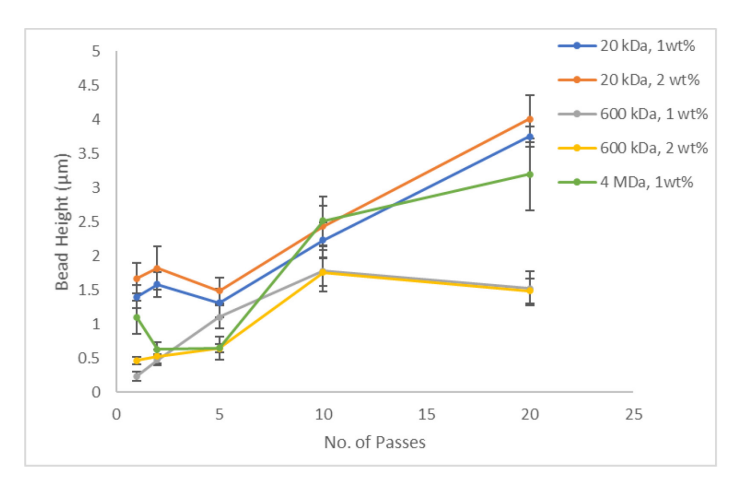


FIGURE 10: INFLUENCE OF PASS COUNT ON BEAD HEIGHT

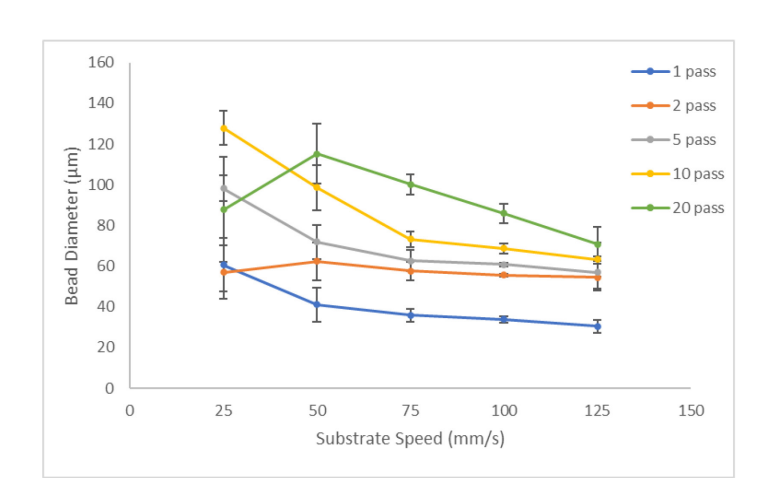


FIGURE 11: INFLUENCE OF SUBSTRATE SPEED ON BEAD DIAMETER

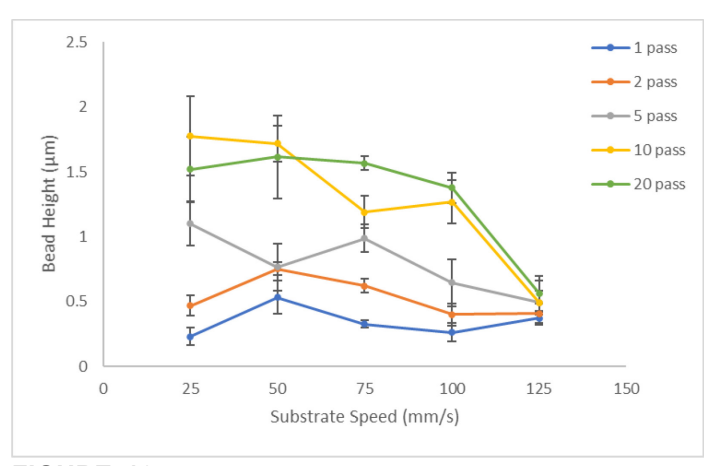


FIGURE 12: INFLUENCE OF SUBSTRATE SPEED ON BEAD HEIGHT

The work presented in this study demonstrates the capabilities of the self-focusing mechanism in NFES and its potential in creating multilayer bead arrays. Since this phenomenon is not well understood, these findings expand the core understanding of this process so that its controllability is tunable. For example, it was revealed that solution chemistry impacts bead morphology while the printing process parameters more so impact the bead size. More work needs to be conducted in order to determine appropriate evaporation times of each solution to better inform the dwell times. Moreover, this manufacturing technique will benefit from strategies to enable bead stacking that avoid adjacent bead coalescence and parallel bead printing during multilayer deposition. These form the core limitations of the self-focusing mechanism, which will be further analyzed in future work. If these limitations are a addressed and overcome, this could serve as a powerful tool for actualizing discrete beaded structures for biomedical and energy applications.

4. CONCLUSIONS

The feasibility of the self-focusing mechanism in EHD printing was demonstrated in this paper. Optimizing process parameters and solution properties allows for tunability in bead morphology and size characteristics. To expand the scope of this research, future studies will focus on improving the reliability of the printed structures and assessing evaporation times and current dissipation methods for different ink formulations. Also, the impact of extensional viscosity will be explored. Solutions in the NFES process undergo high shear rates while being extruded through thin nozzles. It is unclear whether the impact of this is evident through shear rheology. These limitations, if amended, will allow for the self-focusing mechanism to be a powerful, inexpensive, and versatile tool in the manufacturing of multilayer structures that has applications in MEMS and biomedicine.

ACKNOWLEDGEMENTS

The authors would like to thank Emily Ma, Rui Li, and Dr. Nicolas Martinez-Prieto for their contributions to the findings shown in this paper. The authors would also like to acknowledge funding support received from the National Science Foundation Graduate Research Program through Grant No. 1650114,

International Institute for Nanotechnology & Ryan Fellowship, and National Science Foundation Grant No. CMMI 1934350.

REFERENCES

- [1] Al-Qadhi, M., Merah, N., Matin, A., Abu-Dheir, N., Khaled, M., and Youcef-Toumi, K., 2015, "Preparation of Superhydrophobic and Self-Cleaning Polysulfone Non-Wovens by Electrospinning: Influence of Process Parameters on Morphology and Hydrophobicity," Journal of Polymer Research, 22(11).
- [2] Xi, H., and Zhao, H., 2019, "Silk Fibroin Coaxial Bead-on-String Fiber Materials and Their Drug Release Behaviors in Different PH," Journal of Materials Science, **54**(5), pp. 4246–4258.
- [3] Yoon, Y. il, Moon, H. S., Lyoo, W. S., Lee, T. S., and Park, W. H., 2008, "Superhydrophobicity of PHBV Fibrous Surface with Bead-on-String Structure," Journal of Colloid and Interface Science, 320(1), pp. 91–95.
- [4] Li, T., Ding, X., Tian, L., Hu, J., Yang, X., and Ramakrishna, S., 2017, "The Control of Beads Diameter of Bead-on-String Electrospun Nanofibers and the Corresponding Release Behaviors of Embedded Drugs," Materials Science and Engineering C, 74, pp. 471–477.
- [5] Li, D., Wang, M., Song, W. L., Yu, D. G., and Bligh, S. W. A., 2021, "Electrospun Janus Beads-on-a-String Structures for Different Types of Controlled Release Profiles of Double Drugs," Biomolecules, 11(5).
- [6] Zheng, J., He, A., Li, J., Xu, J., and Han, C. C., 2006, "Studies on the Controlled Morphology and Wettability of Polystyrene Surfaces by Electrospinning or Electrospraying," Polymer, 47(20), pp. 7095–7102.
- [7] Huan, S., Liu, G., Han, G., Cheng, W., Fu, Z., Wu, Q., and Wang, Q., 2015, "Effect of Experimental Parameters on Morphological, Mechanical and Hydrophobic Properties of Electrospun Polystyrene Fibers," Materials, **8**(5), pp. 2718–2734.
- [8] Rasouli, M., Pirsalami, S., and Zebarjad, S. M., 2020, "Study on the Formation and Structural Evolution of Beadon-String in Electrospun Polysulfone Mats," Polymer International, **69**(9), pp. 822–832.
- [9] Wong, D., Resendiz, J., Egberts, P., and Park, S. S., 2018, "Electrospinning of Composite Microbeads for Tribological Improvements," Journal of Manufacturing Processes, **34**, pp. 264–273.
- [10] Li, D., Wang, M., Song, W. L., Yu, D. G., and Bligh, S. W. A., 2021, "Electrospun Janus Beads-on-a-String Structures for Different Types of Controlled Release Profiles of Double Drugs," Biomolecules, 11(5).
- [11] Wang, Z., Zhao, C., and Pan, Z., 2015, "Porous Bead-on-String Poly(Lactic Acid) Fibrous Membranes for Air Filtration," Journal of Colloid and Interface Science, **441**, pp. 121–129.
- [12] Shenoy, S. L., Bates, W. D., Frisch, H. L., and Wnek, G. E., 2005, "Role of Chain Entanglements on Fiber Formation during Electrospinning of Polymer Solutions: Good Solvent, Non-Specific Polymer-Polymer Interaction Limit," Polymer, 46(10), pp. 3372–3384.

- [13] Bhat, P. P., Appathurai, S., Harris, M. T., Pasquali, M., McKinley, G. H., and Basaran, O. A., 2010, "Formation of Beads-on-a-String Structures during Break-up of Viscoelastic Filaments," Nature Physics, 6(8), pp. 625– 631.
- [14] Li, J., and Fontelos, M. A., 2003, "Drop Dynamics on the Beads-on-String Structure for Viscoelastic Jets: A Numerical Study," Physics of Fluids, **15**(4), pp. 922–937.
- [15] Rubio, M., Vega, E. J., Herrada, M. A., Montanero, J. M., and Galindo-Rosales, F. J., 2020, "Breakup of an Electrified Viscoelastic Liquid Bridge," Physical Review E, **102**(3).
- [16] Li, F., Ke, S. Y., Yin, X. Y., and Yin, X. Z., 2019, "Effect of Finite Conductivity on the Nonlinear Behaviour of an Electrically Charged Viscoelastic Liquid Jet," Journal of Fluid Mechanics, pp. 5–37.
- [17] Clasen, C., Eggers, J., Fontelos, M. A., Li, J., and McKinley, G. H., 2006, "The Beads-on-String Structure of Viscoelastic Threads," Journal of Fluid Mechanics, **556**, pp. 283–308.

- [18] Liu, Y., He, J. H., Yu, J. Y., and Zeng, H. M., 2008, "Controlling Numbers and Sizes of Beads in Electrospun Nanofibers," Polymer International, 57(4), pp. 632–636.
- [19] Wang, X., Xu, L., Zheng, G., Jiang, J., Sun, D., and Li, W., 2021, "Formation of Suspending Beads-on-a-String Structure in Electrohydrodynamic Printing Process," Materials and Design, 204.
- [20] Lei, T. P., Lu, X. Z., and Yang, F., 2015, "Fabrication of Various Micro/Nano Structures by Modified near-Field Electrospinning," AIP Advances, 5(4).
- [21] Huang, Y., Zheng, G., Xu, L., Sun, D., and Lin, L., 2010, "Bead-on-String Structure Formed by Electrohydrodynamic Printing," 2010 IEEE 5th International Conference on Nano/Micro Engineered and Molecular Systems, NEMS 2010, pp. 537–540.
- [22] Martinez-Prieto, N., Fratta, G., Cao, J., and Ehmann, K. F., 2018, "Deposition of Variable Bead Diameter Arrays by Self- Focusing Electrohydrodynamic Jets," Journal of Micro and Nano-Manufacturing, 6(3).